Oxidation of Metals, Vol. 33, Nos. 1/2, 1990

High-Temperature Corrosion and Mechanical Properties of Protective Scales on Incoloy 800H: The Influence of Preoxidation and Ion Implantation

E. A. Polman,* T. Fransen,*† and P. J. Gellings*

Received February 21, 1989; revised July 20, 1989

Coatings, obtained by preoxidation of Incoloy 800H at low PO_2 show good sulphidation resistance due to the higher chromia content in the oxide scale. Yttrium-ion implantation of Incoloy 800H has also a beneficial effect on sulphidation, if preoxidation is applied. The reason for this is presumably the segregation of yttrium to grain boundaries of the oxide. Furthermore, the oxidation kinetics of Incoloy 800H are independent of the partial pressure of the oxygen. Mechanical testing of the preformed oxide scale/substrate combinations in air at 600°C by means of constant-extension-rate experiments shows that preoxidation at low partial pressures of oxygen leads to earlier scale-cracking.

KEY WORDS: Incoloy 800H; oxidation; sulphidation; ion implantation; CER.

INTRODUCTION

The use of rare earth elements such as cerium, lanthanum, and europium and also additions of yttrium in plasma-sprayed coatings,[1,2] in sol-gel coatings,[1-4] and by ion implantation,[5-8] have been shown to give improved resistance against high-temperature corrosion. Yttrium or cerium, implanted at a dose of 10^{16} to 10^{17} ions/cm^2, also increases the oxidation resistance of chromia-forming alloys.[5-8]

Recently, a beneficial effect of yttrium-ion implantation in Incoloy 800H toward sulphidation was reported.[9,10] The application of an oxidizing pretreatment is essential, since ion-implanted nonpreoxidized samples offer

*Department of Chemical Technology, University of Twente, P.O. Box 217, 7500 AE Enschede, The Netherlands.
†To whom correspondence should be addressed.

0030-770X/90/0200-0135$06.00/0

no protection against sulphidation. It has been shown previously by several authors[1,11] that preoxidation at low-oxygen partial pressures of alumina- and chromia-forming alloys has a beneficial effect on the sulphidation resistance.

In this paper, the composition of the oxide scale after oxidation in oxygen of Incoloy 800H and the distribution of the implanted yttrium in the oxide is reported and discussed in order to better understand the role of yttrium in the corrosion process. Other main issues in this paper are the mechanical behavior and the protective properties of the oxide which is formed after oxidation of Incoloy 800H at various oxygen partial pressures. The determination of the oxide composition is essential in the explanation of the observed effects.

EXPERIMENTAL DETAILS

Incoloy 800H was received as bar material with the following composition: 20 wt.% Cr, 32 wt.% Ni, 1 wt.% Mn, 0.4 wt.% Ti, balance Fe. The material was heat-treated at 1100°C and 950°C, followed by quenching in water of 20°C. The heat-treated bars were machined to cylindrical samples (20 mm length and 5 mm diameter) and disks (12 mm diameter and 2 mm thickness). The cylindrical samples were used to study the oxidation and sulphidation resistance in different atmospheres, and the disks were used for surface analytical investigations. The samples were ground on emery paper to a final size of 4000 grit followed by a polishing treatment on Al_2O_3(0.05 μm). Finally, they were ultrasonically cleaned in ethanol.

Oxidation tests were carried out in a Setaram thermobalance at 900°C and 960°C in pure oxygen, at 900°C in a gas mixture of 1% CO in CO_2, and in a mixture of hydrogen and 1.5 mol % water. The oxygen partial pressures in these mixtures are 1.0×10^{-12} and 9.8×10^{-21} bar, respectively.

Sulphidation tests were carried out in a Cahn-1000 thermobalance in three different atmospheres. At 560°C and at 625°C, argon gas, flowing at a rate of 11 l/hr, was mixed with a gas consisting of 95% H_2 and 5% H_2S, flowing at a rate of 3 l/hr. Another gas mixture was obtained by bubbling the argon through water at 15°C before adding the H_2S, the sulphidation test being carried out at 640°C.

Prior to sulphidation, several preoxidation treatments were applied. The unimplanted samples were oxidized for 1 hr at 960°C. The calculated oxygen and sulphur partial pressures of these gas mixtures are listed in Table I, assuming an oxygen impurity of 1 ppm in the argon.[12]

Cylindrical samples as well as disks were implanted with an energy of 110 keV, using the implantation facility at the University of Groningen. The source used was $Y_2O_3 + CCl_4$.

Table I. Initial Gas Compositions and Calculated Partial Pressures

Medium	Temp (°C)	$\%H_2$	$\%H_2S$	$\%H_2O$	%Ar	Po_2(bar)	Ps_2(bar)
1	560	20.4	1.1	0	bal.	3.8×10^{-36}	1.8×10^{-9}
2	625	20.4	1.1	0	bal.	5.5×10^{-34}	1.2×10^{-8}
3	640	20.4	1.1	1.3	bal.	8.5×10^{-26}	1.7×10^{-8}

Scanning electron microscopy (SEM) and energy dispersive X-ray analysis of the oxide and sulphide scales were performed with a JEOL M35 CF instrument. The phase compositions of the oxide scales were investigated by means of X-ray diffraction.

Semiquantitative analyses of the oxide scales were obtained by XPS analysis on a VG-ESCA3-MK2, using a twin anode of Al and Mg. The spectra obtained after several Ar-sputtering cycles also give information of the binding states of the atoms. The sputter rate was about 60 Å/min.

SIMS analysis was performed on a ARL-IMMA instrument, using N_2^+ ions to make a depth profile of the oxide scale. The sputter time was approximately 50 Å/sec.

Constant-extension-rate (CER) tests were carried out on specimens with a gage diameter of 2.50 mm and an effective gage length of 35.0 mm. The specimens were preoxidized for 3 hr at 900°C using the same atmospheres as mentioned earlier. After 3 hr an oxide thickness of approximately 1 μm was obtained. The CER equipment consisted of a fixed frame, a carriage, a drive mechanism, a load cell, and a recorder. The tests were performed in air at a temperature of 600°C. An extension rate of 4×10^{-7}sec^{-1} was applied. The strain-to-cracking value was determined by scanning electron microscopy after applying the strain.

RESULTS

Oxidation Tests

Oxidation tests of cylindrical samples in pure oxygen (P = 1 bar) at 960°C show that implantation of 10^{16} yttrium ions cm^{-2} in Incoloy 800H, leads to a reduction of the oxidation rate. Both before and after implantation the oxidation behavior is approximately parabolic (see Fig. 1).

The k_p values are $(7.9\pm0.2)\times10^{-12}$ g^{2}cm^{-4}sec^{-1} for the nonimplanted alloy and $(1.6\pm0.1)\times10^{-12}$g^{2}cm^{-4}sec^{-1} for the yttrium-implanted material. For the calculation of the k_p values, the first 30 min of the oxidation were not taken into account.

In order to determine the influence of the oxygen partial pressure on the oxidation behavior, thermogravimetric measurements at 900°C were

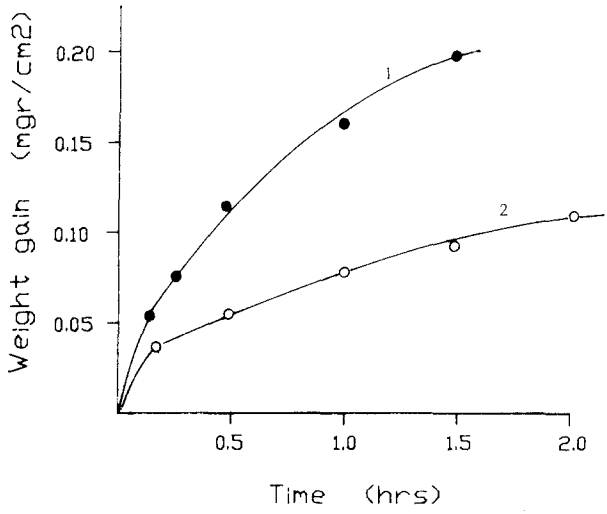

Fig. 1. Oxidation in O_2 at 960°C of Incoloy 800H. 1 = blank; 2 = Y-implanted at a dose of $10^{16}cm^{-2}$.

performed on nonimplanted samples. No significant reduction in oxidation rate is obtained for oxidation of Incoloy 800H at a P_{O_2} of 9.8×10^{-21} bar, compared to oxidation in $CO/CO_2(P_{O_2} = 10^{-14})$ as well as for oxidation in O_2 at 900°C. All oxidation tests show parabolic kinetics. The results of the oxidation tests at various partial pressures are given in Table II.

The oxygen partial pressure independence of the oxidation kinetics was previously observed by Hindam and Whittle for a chromium-nickel alloy at 900°C. The kinetics were only investigated in a small oxygen partial pressure range (from 8×10^{-9} to 2×10^{-14} bar) by using several CO/CO_2 mixtures.[13] Hindam and Whittle also observed that the oxidation kinetics of pure chromium at 1000°C do not depend on the partial pressure. This was also found over a large range of oxygen pressures at 900°C by the present authors and will be published in a subsequent paper.[14]

Table II. K_p Values in $g^2cm^{-4}sec^{-1}$

Sample	Temp (°C)	atm.	$k_p(\times 10^{+12})$
Incoloy 800H	960	O_2	7.9 ± 0.2
Incoloy impl. 10^{16} Ycm^{-2}	960	O_2	1.6 ± 0.1
Incoloy 800H	900	O_2	2.0 ± 0.2
Incoloy 800H	900	CO/CO_2	2.6 ± 0.1
Incoloy 800H	900	H_2/H_2O	1.5 ± 0.4

Several oxidation tests were performed at 900°C in H_2/H_2O by oxidizing many samples simultaneously, without registering the weight gain during the oxidation. After 20 hr, the ratio of the weight gain of the implanted specimens compared to the nonimplanted samples was 1:2.5. This experiment showed that yttrium-ion implantation in Incoloy 800H leads to a decrease in the oxidation rate over a large range of oxygen pressures.

Sulphidation Tests

Prior to sulphidation, several preoxidation treatments were applied. The unimplanted samples were oxidized for 1 hr at 960°C and the yttrium-implanted specimens were oxidized for 4 hr at this temperature in order to obtain a similar oxide layer thickness of about 1 μm. At low oxygen partial pressures all samples were preoxidized for 20 hr at 900°C.

The sulphidation was stopped after a weight gain of approximately 1 mg/cm^2 was reached. At this weight gain the oxide coatings can no longer be regarded as protective and the mass transport is mainly governed by locally formed sulphide ducts.

If Incoloy 800H is not preoxidized at all very poor sulphidation resistance is obtained as shown by Fig. 2 (curve 1). For yttrium-implanted nonpreoxidized samples, the same poor sulphidation resistance is observed (see also curve 1). Preoxidation results in the formation of a protective oxide coating (curve 2).

Preoxidation in oxygen of yttrium-ion-implanted samples results in better sulphidation resistance, compared to blanks (see curve 3). The sulphidation tests in medium 1 (Fig. 2, curve 3) and medium 3 (Fig. 4, curve 3) show that the corrosion rate is decreased by a factor of 5–10.

Preoxidation at a low oxygen partial pressure leads to much better sulphidation resistance than preoxidation in oxygen. For preoxidation in H_2/H_2O the sulphidation behavior is even better than for samples preoxidized in CO/CO_2 (see Fig. 2, curves 5 and 4 respectively). The blank samples preoxidized in H_2/H_2O and exposed in medium 1 (Fig. 2, curve 5) and the blank and implanted samples, preoxidized in H_2/H_2O and sulphidized in medium 3 (Fig. 4, curves 2 and 4) showed no weight gain after 150 hr and 250 hr, respectively. SEM-observations made clear that there was only a very slight localized attack by sulphur.

No difference was observed in corrosion behavior between implanted and nonimplanted samples, preoxidized at low oxygen partial pressures during sulphidation in medium 2 (Fig. 3, curves 2 and 3). The large deviation between the duplicate measurements in Fig. 3 (curves 2 and 3) may be due to the very severe corrosive atmosphere. Once the protective scale is affected, sulphidation proceeds at a high rate, and small differences in attacked area may then cause large differences in weight change.

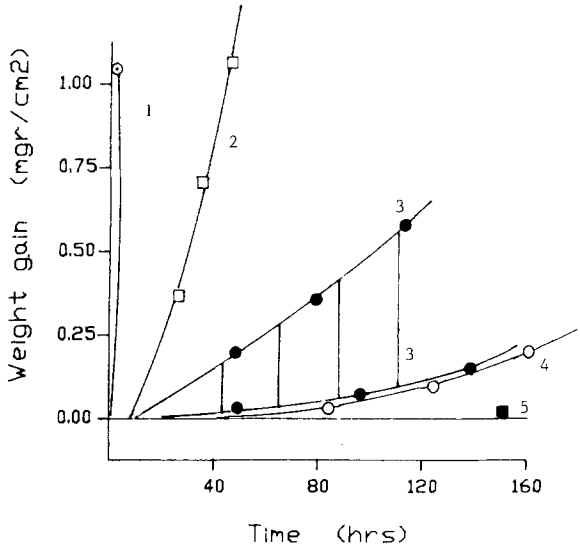

Fig. 2. Sulphidation in medium 1. 1 = blank nonpreoxidized; 2 = blank preoxidized in O_2; 3 = 10^{16}Ycm^{-2} preoxidized in O_2; 4 = blank preoxidized in CO/CO_2; 5 = blank preoxidized in H_2/H_2O.

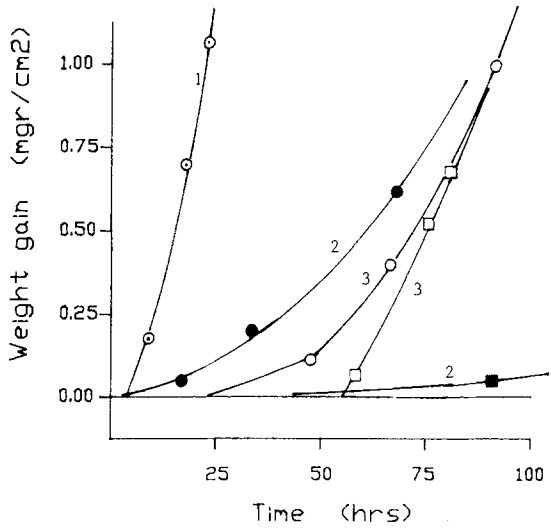

Fig. 3. Sulphidation in medium 2. 1 = blank preoxidized in O_2; 2 = blank preoxidized in H_2/H_2O; 3 = 10^{16}Ycm^{-2} preoxidized in H_2/H_2O.

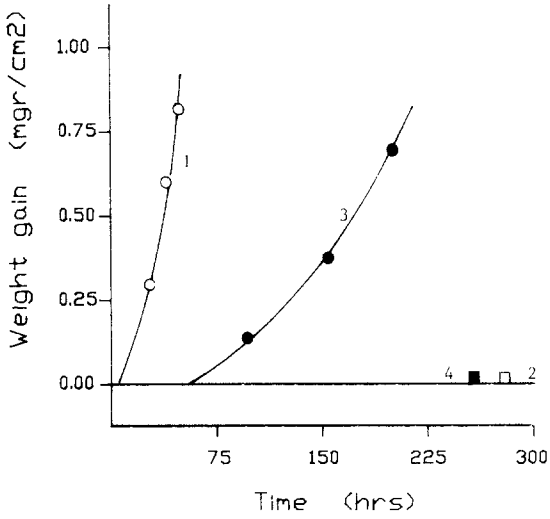

Fig. 4. Sulphidation in medium 3. 1 = blank preoxidized in O_2; 2 = blank preoxidized in H_2/H_2O; 3 = 10^{16}Ycm^{-2} preoxidized in O_2; 4 = 10^{16}Ycm^{-2} preoxidized in H_2/H_2O.

CER Experiments

The CER tests performed at 600°C in air show that the strain-to-cracking of preoxidized scales is influenced by the preoxidizing conditions. For preoxidation in O_2, the strain-to-cracking is 1.5%, whereas preoxidation in 1% CO/CO_2 as well as in 1.5% H_2O/H_2 leads to a strain-to-cracking of 0.75%.

It was possible to detect the formation of small cracks by means of SEM. The cracks propagate perpendicular to the tensile direction. An example of a cracked oxide scale is given in Fig. 15. The oxide was formed at 900°C in 1% CI/CO_2 and the total strain was 1%. If cracking occurred, several cracks could be observed.

SIMS Measurements

By means of SIMS, small changes in concentrations of elements present at low concentrations can be determined. Because of the strong matrix effects, SIMS can only be used as a quantitative technique if a set of well-defined standards is available.

SIMS spectra of a blank and an implanted sample, both with an oxide thickness of about 1 μm and both oxidized at 960°C in oxygen, are shown in Figs. 5 and 6. For silicon and aluminum, which are both present in

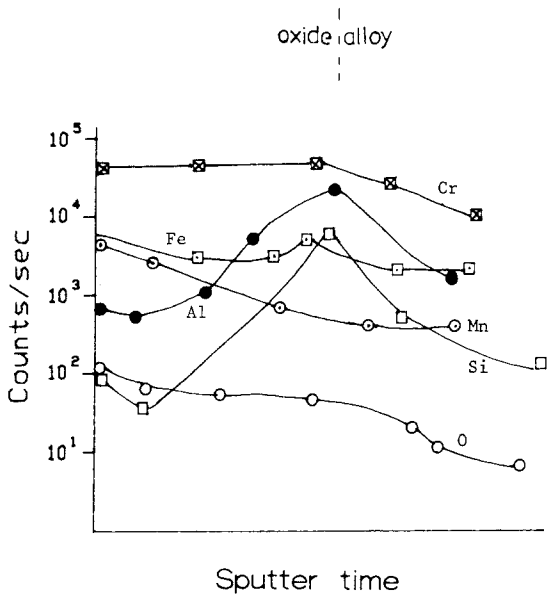

Fig. 5. SIMS depth profile for Incoloy 800H oxidized in O_2 at 960°C for 1 hr.

amounts of a few tenths of a percent in the alloy, a maximum in concentration at the oxide/alloy interface is observed. Probably these elements are preferentially oxidized during the first stages of the oxidation due to their high affinity for oxygen.[15]

The yttrium in the oxide of the implanted alloy also has a maximum at the oxide/alloy interface. This is in disagreement with the conclusions drawn from previous Rutherford Back Scattering measurements.[10] It is possible that small amounts of Cu or Mo in the outer oxide give rise to the observed RBS spectrum, since Cu and Mo are both present in the alloy in small amounts.

XPS Measurements

The XPS measurements were used to determine a depth profile by sputtering with argon. In measuring depth profiles, selective-sputtering effects must be taken into account. Also the oxide of Incoloy 800H cannot be regarded as a smooth regular surface (Fig. 11). However, changes in concentration can still be observed, and comparisons between different samples of Incoloy 800H are also possible.

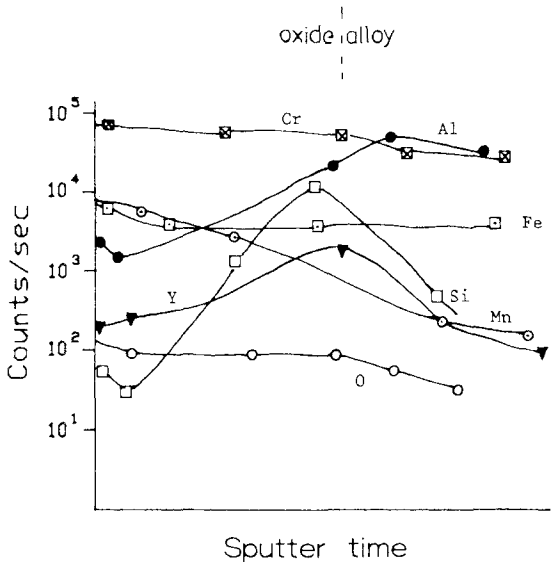

Fig. 6. SIMS depth profile for Y-implanted Incoloy 800H, preoxidized in O_2 at 960°C for 3 hr.

To quantify the spectra, obtained by using Al-K_a radiation, the peak areas of the strong XPS signals were measured. The sensitivity factors for the peak areas were taken from Jørgensen and Berthou[16] which differ in some respects from those published later by Wagner *et al.*,[17] but give more consistent results for the bulk of Incoloy 800H, used as a standard. Corrections for interfering Auger peaks were made by also measuring some peaks with a Mg-K_a radiation source. For the Mg-K_a radiation, the sensitivity factors of Berthou and Jørgensen[18] were also used.

The depth profiles obtained for a blank specimen oxidized in O_2 at 960°C for 1 hr, one oxidized in H_2/H_2O at 900°C and a yttrium-implanted specimen oxidized in O_2 at 960°C for 4 hr, respectively, are plotted in Figs. 7–9. The oxide/alloy interface was not very sharp due to sputtering effects and the irregularity of the interface. The position of the interface was determined by an increase in the iron and nickel contents and a slight decrease in the oxygen content.

The yttrium concentration in the oxidized implanted Incoloy 800H is observed to be high in the oxide at the oxide/alloy interface, but the yttrium is also present in low amounts all over the oxide scale.

The overall compositions of the oxides of the implanted and the nonimplanted alloy, oxidized in O_2, are quite similar. Aluminum and

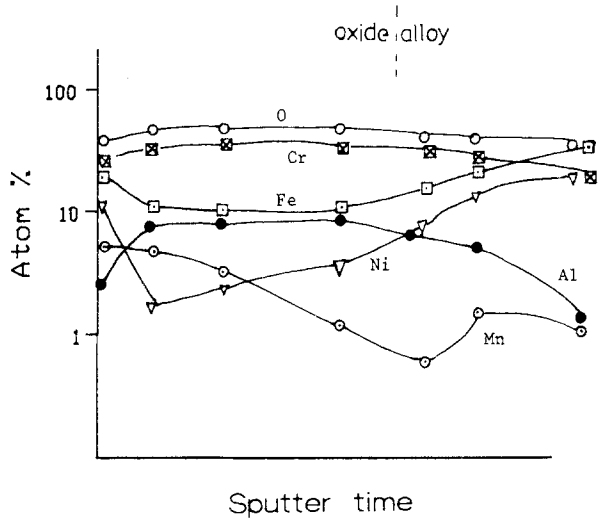

Fig. 7. XPS depth profile for Incoloy 800H preoxidized in O_2 at 960°C for 1 hr.

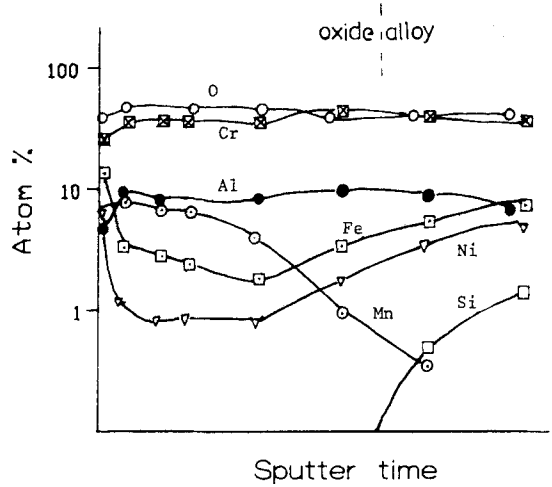

Fig. 8. XPS depth profile for Incoloy 800H preoxidized in H_2O/H_2 at 900°C for 20 hr.

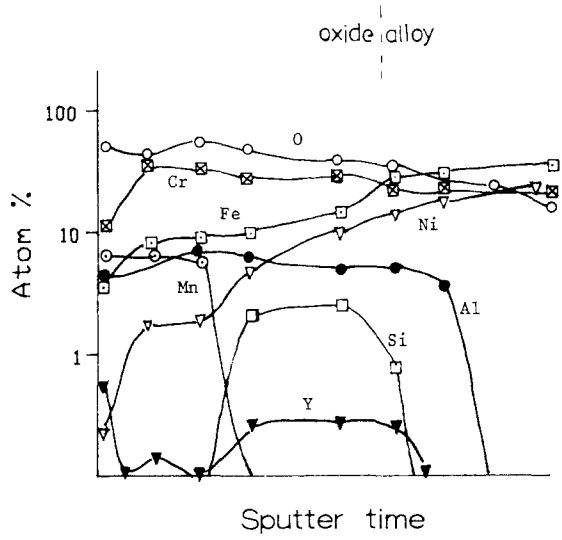

Fig. 9. XPS depth profile for Incoloy 800H, Y-implanted, preoxidized in O_2 at 960°C for 3 hr.

manganese are both preferentially oxidized, and aluminum and silicon again show maximum concentrations at the oxide/alloy interface. Chromium oxide is the main component in the oxide scale.

The oxide scale of the blank specimen oxidized in H_2/H_2O shows higher concentrations of chromium, aluminum, and manganese, compared with the samples oxidized in O_2. This can be understood easily if the thermodynamic stability of the compounds under the oxidation conditions is taken into account.[15] Chromium, aluminum, manganese, and silicon are the only elements which have stable oxide phases according to thermodynamics under these conditions. As a consequence nickel- and iron-oxide are present in lower amounts than in the oxide formed by oxidation in O_2.

XRD Measurements

XRD measurements were performed on oxide scales grown on Incoloy 800H at 900°C in O_2 as well as in H_2/H_2O. Incoloy 800H was oxidized for 2 hr, resulting in an oxide thickness of about 1 μm.

The ratio of the surface areas of the Cr_2O_3 (104) reflection compared to the spinel (311) reflection was found to be two for both oxide types. It is understandable that at least the oxide grown in H_2O/H_2 will have a lower Fe and Ni and a higher Al and Mn content, because at low P_{O_2} the preferential oxidation of Al and Mn is larger than at higher P_{O_2}. Since

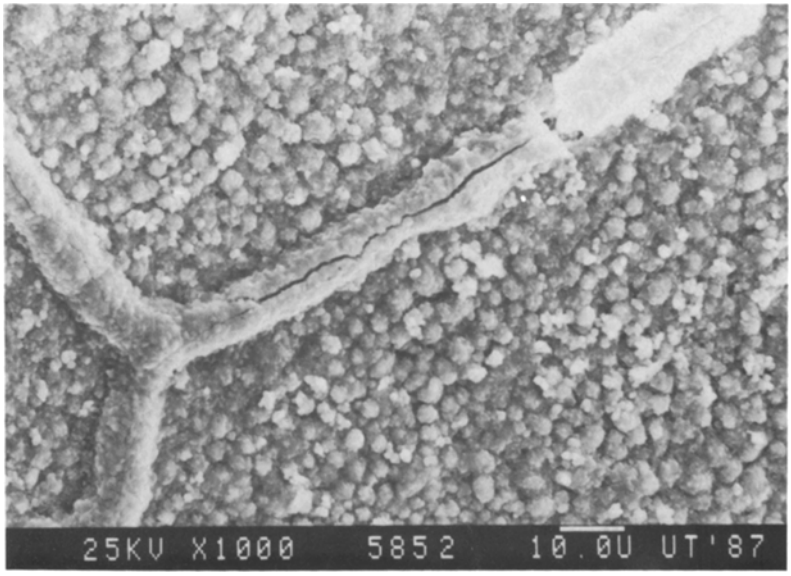

Fig. 10. Incoloy 800H oxidized in O_2 at 960°C for 1 hr.

XRD does not very easily allow to distinguish between the various spinel compositions, the spectra give no further information about the oxide composition.

SEM Observations

The surface of blank specimens oxidized in O_2 and of a specimen oxidized in H_2/H_2O in Fig. 10–13, respectively. The oxide obtained after oxidation in H_2/H_2O is less porous on the outside, and the outer grains are locally mutually attached.

The sample shown in Fig. 14 was preoxidized in H_2/H_2O and sulphidized for 290 hr in medium 3 and shows only localized attack by sulphur at the thicker oxide present on the alloy grain boundaries which have been mentioned earlier as fast-diffusion paths.[10] Figure 15 gives an example of a cracked oxide scale. The cracking was observed at a strain of 1% at 600°C after preoxidation in 1% CO/CO_2 at 900°C.

DISCUSSION

Oxidation and Sulphidation Behavior

Several mechanisms have been proposed to account for the beneficial effect of rare-earth elements in alumina- or chromia-forming oxide scales.

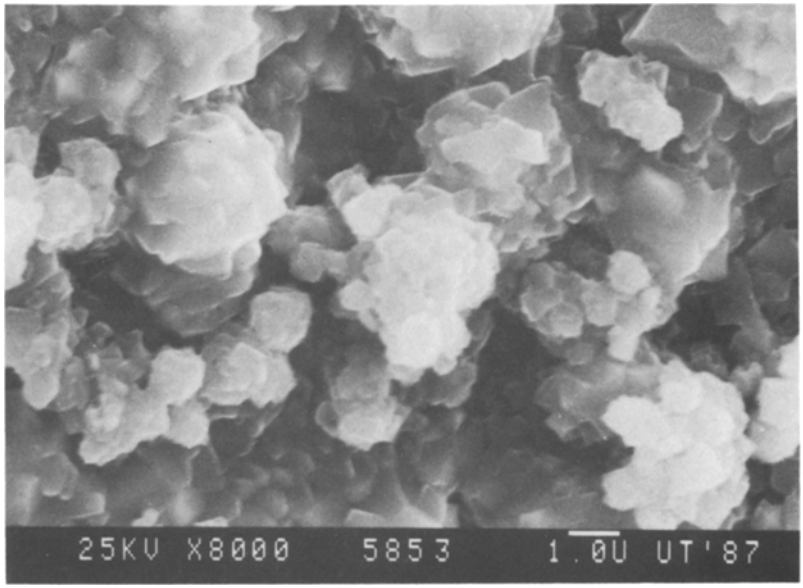

Fig. 11. Incoloy 800H oxidized in O_2 at 960°C for 20 hr (higher magnification of Fig. 10).

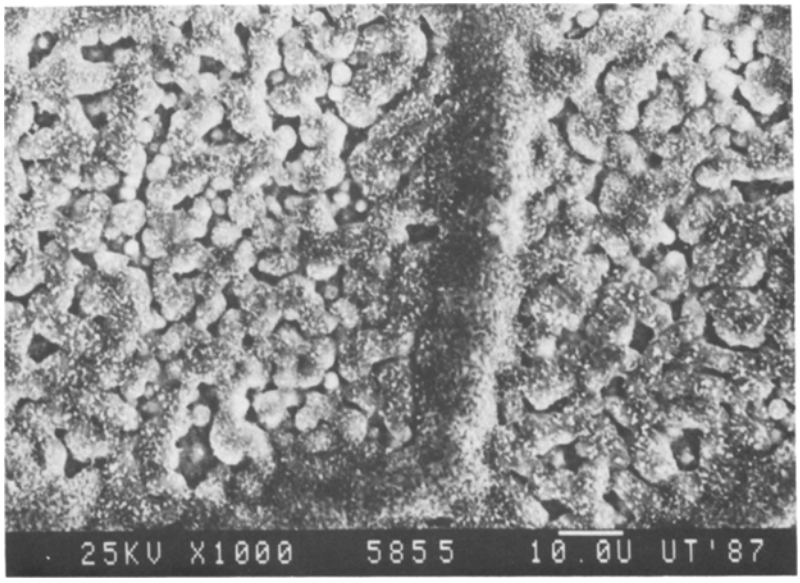

Fig. 12. Incoloy 800H oxidized in H_2O/H_2 at 900°C for 20 hr.

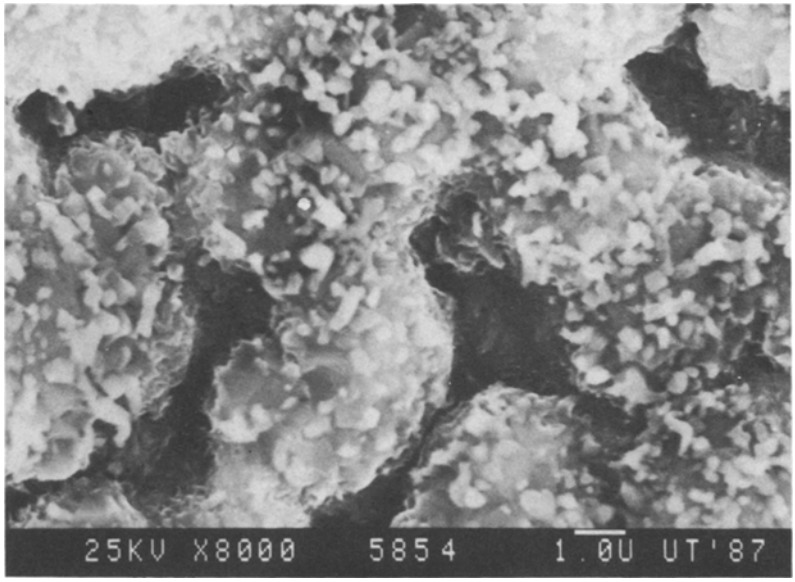

Fig. 13. Incoloy 800H oxidized in H_2O/H_2 at 900°C for 20 hr (higher magnification of Fig. 12).

These mechanisms were reviewed by Whittle and Stringer[19] and recently by Moon.[20] The effects caused by the proposed mechanisms can generally be divided in three groups:

1. The effects on the initial oxidation.
2. The prevention of scale failure.
3. The reduction of the growth rate.

Effects on Initial Oxidation

According to Stringer,[21] chromia grains nucleate on rare-earth dispersoids, thus forming a closed chromia layer and reducing the normally needed amount of chromium in the alloy. The SIMS and especially the XPS results in this work show that the mean compositions of the oxide on the yttrium-implanted alloy and on the blank are about the same, and that the chromium contents near the alloy/oxide interface in the oxide are very high for both samples. Therefore, it is not likely that the formation of a chromia layer in the initial stages of oxidation is playing a significant role. Also, the model is not applicable for the explanation of the beneficial effect of yttrium-ion implantation in pure chromium as observed by Cotell and Yurek.[22]

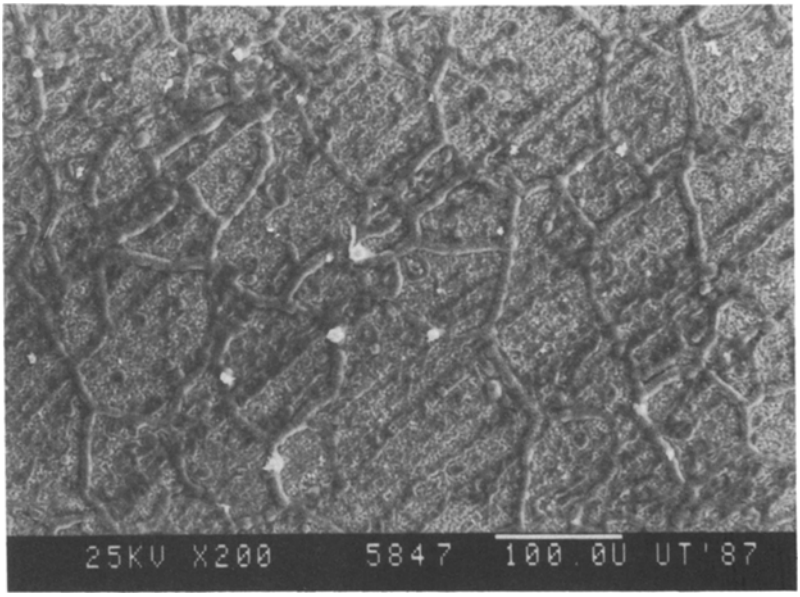

Fig. 14. Incoloy 800H, preoxidized in H_2O/H_2 for 20 hr, sulphidized for 290 hr in medium 3. The white spots are sulphides formed on oxide grain-boundary ridges.

Prevention of Scale Failure

Scale failures such as spalling can drastically be diminished by the additions of rare-earth elements, and several mechanisms were proposed to explain this improved behavior. However, oxide spalling never occurred for the oxide scales of the yttrium-implanted as well as for the nonimplanted Incoloy 800H, as shown by the sensitive thermogravimetric experiments and by the SEM observations. Therefore, the prevention of scale failure does not play a role in the improved isothermal oxidation resistance of yttrium-implanted Incoloy 800H.

Reduction of Growth Rate

In the applied corrosion tests, the blocking of fast-diffusion paths seems the only reasonable mechanism. Atkinson has shown by means of chromium-tracer-diffusion experiments on chromia single crystals that the chromium lattice diffusion in chromia can never account for the observed oxidation rates.[23] Therefore, the main transport mechanism in oxide scales on chromium and chromia-forming alloys must take place by means of fast diffusion paths such as grain boundaries. The effect of rare-earth elements on scale growth is thus generally assumed to be due to the reduction of

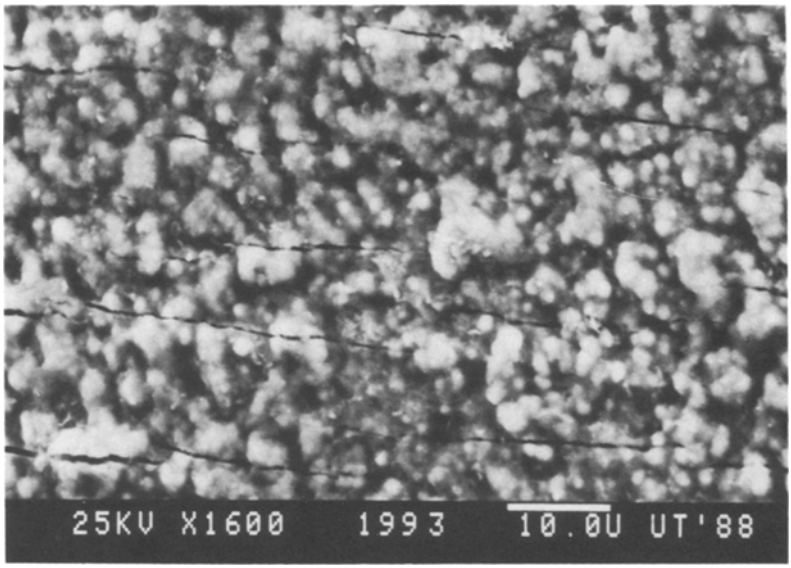

Fig. 15. Cracked oxide after application of 1% strain in air; the oxide was preformed in CO/CO_2 at 900°C.

grain-boundary diffusion. Experimental support for this theory was recently given by Przybylski and Yurek who observed yttrium segregation at the boundaries of chromia grains on a yttrium-implanted cobalt-chromium alloy.[24] The experiments of Cotell and Yurek for Y-implanted chromium show that the cation diffusion is more affected than the oxygen transport in the protective scale.[22] Both the distribution of oxygen tracer and of the yttrium in the oxide scale after oxidation at 900°C show that the ratio between the oxygen and metal diffusion in the oxide scale is increased by implantation.

The exact mechanism by which rare-earth elements hinder the transport at the grain boundaries is not clear. Przybylski and Yurek suggested that the reduction of the available chromium sites at the grain boundaries might reduce the chromium transport. The diffusion of doped chromia could then be described by:

$$D_{Cr}(gb) = a_{Cr} \times D^0_{Cr}(gb) \times \delta \tag{1}$$

where $D^0_{Cr}(gb)$ is the grain-boundary diffusion coefficient for chromium cations in pure chromia, δ is the grain boundary width, and $D_{Cr}(gb)$ is the diffusion coefficient for chromium cations in yttrium-doped chromia.[24] Although there is no direct evidence for this to occur, it cannot be excluded

as long as the chromium concentration at the outer layers of the grain boundary is not exactly known.

The transport along grain boundaries may also be affected by a decrease of the chromium-defect concentration due to yttrium doping. El-Aiat and Kröger proposed yttrium to act as an isoelectronic donor in alumina due to its large radius.[25] As a result of the donor action of a yttrium ion occupying an aluminum lattice site, the concentration of the aluminum interstitials, assumed to be the majority of aluminum defects, should decrease. Ramanarayanan and Petkovic-Luton proposed that for yttrium addition, to chromia-forming alloys a similar mechanism may occur.[26] However, this mechanism is very speculative, since the defect chemistry of chromia grown on chromium at the usual oxidation temperatures (900–1100°C) is not clear.[27]

The reduction in oxidation rate for yttrium-implanted Incoloy 800H at 960°C corresponds well with the findings of Bennett *et al.* for yttrium-implanted 20Cr–25Ni–Nb stabilized steel at 950°C.[28] At higher temperatures the effectiveness of yttrium implantation even increases as shown by Bennett *et al.*[28] and Przybylski and Yurek.[24]

SIMS and XPS show that for yttrium-implanted Incoloy 800H, the maximum of the yttrium distribution is in the oxide near the alloy/oxide interface. Assuming yttrium to act as a marker, the yttrium distribution shows that the main transport mechanism during oxidation is still cation diffusion, and the reduction of the oxidation rate can therefore only be explained by means of a decreasing cation transport along grain boundaries.

In the case of sulphidation, the effect of yttrium in the preformed oxide is not clear. It was previously stated that yttrium implantation is most effective in the case of oxidation at high temperatures. Evidence for this was presented by Bennett who measured a slightly lower energy of activation for the oxidation of yttrium-implanted 20Cr–25Ni–Nb stabilized steel compared to nonimplanted steel.[27] Therefore, it is not likely that the blocking of cation diffusion along grain boundaries is very effective at the temperatures of sulphidation (550–650°C). Possibly the attack by sulphurous gas species, or sulphur transport along oxide grain boundaries, which is assumed to be the first step in the sulphur transport through oxide scales because of the limited metal diffusion at these temperatures, is affected by rare-earth elements. When the sulphidation does proceed, the sulphidation kinetics are governed by outward metal transport through the sulphide scales formed or sulphide ducts.

The sulphidation tests of Incoloy 800H show that a decrease in the partial oxygen pressure of the preoxidizing atmosphere gives an improvement in the sulphidation behavior. It is likely that a closed chromia layer is formed. The oxide is therefore less easily converted to sulphides. The

XPS sputtering profiles show only a slight increase of the chromium content after preoxidation at low partial pressure. This may mean that the structure of the oxide shows less defects due to its higher stability.

The Mechanical Behavior

Strain-to-cracking of oxide scales can occur due to one or more of the following contributions:

1. Lateral oxide growth, giving rise to crack healing.
2. Elastic deformation.
3. Plastic deformation.

Lateral Oxide Growth

Schütze derived the following equation for the healing rate of the oxide:

$$E_0 h = 2k_p / l_r \cdot x \tag{2}$$

where $E_0 h$ is the critical strain rate, k_p the parabolic rate constant, x the distance between the crack face and the metal, and l_r the distance between the oxide cracks.[29]

A rough estimate of $E_0 h$, obtained by taking k_p as 3.4×10^{-20} $m^2 sec^{-1}$ at 600°C found by means of extrapolation of k_p values obtained at higher temperatures,[30] l_r as 10 μm, and x as 1 μm, shows that crack-healing by means of lateral oxide growth can occur only below a strain rate of 7×10^{-9} sec^{-1}. The effect of lateral oxide growth at the applied strain rate of 4×10^{-7} sec^{-1} can therefore be neglected.

Elastic Deformation

Only few data are available for the elastic behavior of chromia scales. Schütze estimated that the purely elastic deformation of chromia scales would amount to about 0.09%.[31] This was based on the values for sintered alumina[32] and measurements of the elastic modulus for chromia scales.[33]

Plastic Deformation

According to creep experiments of Burton and Reynolds,[34] chromia shows plastic behavior above 1200°C. These measurements were performed on large-grain, high-density chromia rods, sintered at 1600°C.

In no. 1 it was shown that the absence of strain-to-cracking of the preformed oxide scales up to at least 0.75% can certainly not be accounted for by lateral oxide growth. The contribution of the elasticity and plasticity of the 1-μm thick oxide scales might be significantly higher than the values assumed in nos. 2 and 3.

Kofstad showed that 50-μm thick, fine-grain chromia scales, formed at 1000°C in 10^{-7} bar O_2, have an enormous ability to deform without cracking.[35] The scales detach and balloon away from the metal. Fine-grain chromia scales may therefore also deform plastically at moderate temperatures (600–900°C) due to grain-boundary sliding.

All values in this work for strain-to-cracking are significantly higher than the values found by Schütze for oxide scales formed on Incoloy 800H at 800°C.[31] The cross-sections of the oxide scales show that the measurements of Schütze were performed on much thicker oxide scales of approximately 15 μm. These thicker oxide scales probably show less stress relaxation than the oxide scales investigated in this work, since Evans *et al.* showed that the stress relaxation for coatings on a substrate is inversely related to the coating thickness and the grain size.[36]

The reason for the much lower strain-to-cracking values observed for the scales preoxidized at low P_{O_2} is not quite clear. From Fig. 11 and 12 it is obvious that scales preoxidized in H_2/H_2O show more pronounced grain-boundary oxidation than scales formed in O_2, leading to locally attached grains forming aggregates which are likely to admit less grain-boundary sliding and therefore less scale plasticity, in agreement with the observed scale-cracking behavior.

Another possible explanation is derived from the experiments of Howes and Richardson who observed large tensile stresses on strips of Fe–Cr steel, selectively oxidized at one side.[37] The tensile stresses for a Fe–20Cr alloy were larger than for Fe–28Cr and Fe–16Cr steel. Howes and Richardson attribute the tensile stresses to the formation of Cr_2O_3 on top of the initially formed Fe-rich oxide. The difference in molecular volume of Fe_2O_3 compared to Cr_2O_3 gives rise to tensile stress. Howes and Richardson showed that a small change in the ratio Fe_2O_3:Cr_2O_3 may result in a large increase in tensile stress. It is possible that oxidation of Incoloy 800H at low P_{O_2}, giving rise to a chromium-enriched oxide, results in larger tensile stresses than oxidation at high P_{O_2}. However, this theory is speculative, since it has not been verified whether the stresses in the oxide layer are compressive or tensile. An exact estimate of the change in composition of the oxide would also require a more precise determination of the oxide composition near the alloy/oxide interface. Due to selective-sputtering effects and the curved oxide/alloy interface, it is hard to obtain this information from the measured XPS spectra.

CONCLUSIONS

- Preoxidation of Incoloy 800H in a mixture of H_2/H_2O is very effective in reducing the sulphidation rate.

- Yttrium-ion implantation of Incoloy 800H effectively reduces the oxidation rate and reduces the sulphidation rate if preoxidation at high P_{O_2} is applied after implantation.
- The observed oxidation and sulphidation behavior of yttrium-implanted Incoloy 800H may be due to the blockage of short-circuit diffusion paths.
- 1-μm thick oxide scales of Incoloy 800H show a large strain-to-cracking value due to increased elastic and/or plastic deformation. The smaller strain-to-cracking values for CER experiments on scales formed at low P_{O_2} are suggested to be due to selective oxide grain-boundary growth.

ACKNOWLEDGMENTS

The University of Groningen provided the implantation facility. We particularly wish to thank J. Smit for ion implanting the specimens. Dr. E. G. Keim is acknowledged for the XPS spectra measured at the University of Twente. The SGM foundation is thanked for putting their SIMS facility at our disposal. D. Gras is especially thanked for his assistance.

REFERENCES

1. T. Fransen, M. M. A. Perik, H. Fikkert, M. A. de Jongh, and P. J. Gellings, 8th. European Corrosion Congress Nice 53-1 (1985).
2. T. Fransen, E. A. Polman, M. M. A. Perik, and P. J. Gellings, Proceedings "International Congress for High Temperature Alloys and other Gas Applications" Liege 1173 (1986).
3. T. Fransen, M. A. de Jongh, M. M. A. Perik, and P. J. Gellings, *Proc. 9th Internat. Congress Metal. Corros. Toronto* **4**, 311 (1984).
4. T. Fransen, P. J. Gellings, J. C. Fuggle, G. van der Laan, J. M. Esteva, and R. C. Karnatak, *Appl. Surface Sci.* **20**, 257 (1985).
5. M. J. Bennett, G. Dearnaley, M. R. Houlton, R. W. M. Hawes, P. D. Goode, and M. A. Wilkins, *Corrosion Sci.* **20**, 73 (1980).
6. M. J. Bennett, G. Dearnaley, M. R. Houlton, and R. W. M. Hawes, in V. Ashworth, W. A. Grant, and R. P. M. Procter (eds.), *Proceedings of the Conference On Ion Implantation into Metals* (Pergamon, Oxford, 1982), p. 264.
7. M. J. Bennett, B. A. Bellamy, C. F. Knights, N. Meadows, and N. J. Eyre, *Mat. Sci. Engin.* **69**, 359 (1985).
8. J. C. Pivin, C. Roques-Carmes, J. Chaumont, and H. Bernas, *Corrosion Sci.* **20**, 359 (1980).
9. J. H. Kort, T. Fransen, and P. J. Gellings, *Appl. Surface Sci.* **25**, 237 (1986).
10. E. A. Polman, T. Fransen, and P. J. Gellings, *Mat. Sci. Engin.* **88**, 157 (1987).
11. F. H. Stott, F. M. F. Chong, and C. A. Stirling, *9th Internat. Congress Metal. Corros.* **2**, 1 (1984).
12. P. J. Gellings, internal report.
13. H. Hindam and D. P. Whittle, *J. Electrochem. Soc.* **130**, 1519 (1983).
14. E. A. Polman, T. Fransen, and P. J. Gellings, to be published.
15. I. Barin and C. Knacke, in *Thermodynamical Properties of Inorganic Substances* (Springer-Verlag, Berlin, 1973).
16. C. K. Jørgensen and H. Berthou, *J. Chem. Soc. Faraday Discuss.* **54**, 269 (1954).

17. C. D. Wagner, L. E. Davids, M. V. Zeller, J. A. Taylor, R. M. Raymond, and L. H. Gale, *Surf. Interface Anal.* **3**, 211 (1981).
18. H. Berthou and C. K. Jørgensen, *Analyt. Chem.* **47**, 482 (1975).
19. D. P. Whittle and J. Stringer, *Phil. Trans. Royal Soc. London* **A295**, 309 (1980).
20. D. P. Moon and M. J. Bennett, AERE report R 12757.
21. J. Stringer and I. G. Wright, *Oxid. Met.* **5**, 59 (1972).
22. C. M. Cotell, G. J. Yurek, R. J. Hussey, D. F. Mitchell, and M. J. Graham, *J. Electrochem. Soc.* **134**, 1871 (1987).
23. A. Atkinson and R. I. Taylor, *NATO ASI Series B* **129**, 285 (1984).
24. K. Przybylski, A. J. Garratt-Reed, and G. J. Yurek, *J. Electrochem. Soc.* **135**, 509 (1988).
25. M. M. El-Aiat and F. A. Kröger, *J. Am. Ceramic Soc.* **66**, C-202, (1983).
26. T. A. Ramanarayanan and R. Petkovic-Luton, *Berichte der Bunsengeschellschaft der Physische Chemie* **89**, 402 (1985).
27. E. A. Polman, T. Fransen, and P. J. Gellings, *J. Physics C* (in press).
28. M. J. Bennett, H. E. Bishop, P. R. Chalker, and A. T. Tuson, *Mat. Sci. Engin.* **90**, 177 (1987).
29. M. Schütze, *Oxid. Met.* **25**, 409 (1986).
30. J. C. Langevoort, thesis, University of Twente (1985).
31. M. Schütze, *Oxid. Met.* **24**, 199 (1985).
32. G. V. Samsonow, ed., *The Oxide Handbook* (IFI/Plenum, New York, 1973).
33. R. C. Hurst and P. Hancock, *Korrosion* **24**, 33 (1973).
34. B. Burton and G. L. Reynolds, *J. Mat. Sci.* **13**, 219 (1978).
35. P. Kofstad and K. P. Lillerud, *J. of the Electrochem. Soc.* **127**, 2410 (1980).
36. A. G. Evans, G. B. Crumley, and R. E. Demaray, *Oxid. Met.* **20**, 193 (1983).
37. V. R. Howes and C. N. Richardson, *Corrosion Sci.* **9**, 385 (1969).